Check for updates

UCN–SiO$_2$–GO: a core shell and conjugate system for controlling delivery of doxorubicin by 980 nm NIR pulse†

Pradip Paik, [ID] *[ab] K. Santhosh Kumar,[b] Monami Das Modak,[b] Koushi Kumar U[b] and Somedutta Maity[ab]

Herein, graphene oxide (GO) has been attached with core–shell upconversion-silica (UCN–SiO$_2$) nanoparticles (NPs) to form a GO–UCN–SiO$_2$ hybrid nanocomposite and used for controlled drug delivery. The formation of the nanocomposite has been confirmed by various characterization techniques. To date, a number of reports are available on GO and its drug delivery applications, however, the synergic properties that arise due to the combination of GO, UCNPs and SiO$_2$ can be used for controlled drug delivery. New composite UCN@SiO$_2$–GO has been synthesized through a bio-conjugation approach and used for drug delivery applications to counter the lack of quantum efficiency of the upconversion process and control sustained release. A model anticancer drug (doxorubicin, DOX) has been loaded to UCNPs, UCN@SiO$_2$ NPs and the UCN@SiO$_2$–GO nanocomposite. The photosensitive release of DOX from the UCN@SiO$_2$–GO nanocomposite has been studied with 980 nm NIR laser excitation and the results obtained for UCNPs and UCN@SiO$_2$ NPs compared. It is revealed that the increase in the NIR laser irradiation time from 1 s to 30 s leads to an increase in the amount of DOX release in a controlled manner. *In vitro* studies using model cancer cell lines have been performed to check the effectiveness of our materials for controlled drug delivery and therapeutic applications. Obtained results showed that the designed UCN@SiO$_2$–GO nanocomposite can be used for controlled delivery based therapeutic applications and for cancer treatment.

Introduction

Upconversion nanoparticles (UCN) convert low-frequency light into high-frequency light. This phenomenon was observed in 1960 by Auzel Ovsyankin and Feofilov.[1] UCN NPs are used in various applications including fluorescent imaging for cancer diagnostics[2] and photodynamic therapy for treatment (PDT).[3–6] These UCN materials can be inorganic or organic/polymer materials.[7] Inorganic UCN materials can be synthesized through thermal treatment of inorganic precursors, whereas polymer based UCN materials can be synthesized through various polymerization techniques, such as reversible addition fragmentation chain transfer (RAFT), ring opening polymerization (ROP) *etc.*[8] With these polymers NIR light sensitive cyano-based dyes can be conjugated. In PDT, after excitation by NIR laser light, UCN release drug/medicines loaded in the nanocapsules of polymers of inorganic materials.[9] During this process, NIR excites lower state electrons to the higher energy levels and subsequently converts lower-energy light to higher-energy light and influences the release of drugs at the targeted sites. However, the efficiency of the PDT process depends on the constituent materials (*e.g.*, polymer, peptide, hydro gel *etc.*) and loaded photosensitizer.[10] PDT has several advantages over more conventional cancer therapies such as, it is cost effective, able to treat/kill the infected cells at highly localized sites and is specific for tumor treatments and exhibits a higher cure rate for some tumors.[5,6,9]

To date, a number of reports are available on the application of GO for drug delivery [11–13] However, the loading of drug in GO is influenced by its electronic structure and electronic environment. A number of nanoparticles including UCN NPs are also reported for drug delivery and cancer therapy.[14–16] To the best of our knowledge, a nanocomposite of GO conjugated with UCN@SiO$_2$ NPs and its role in sustained drug delivery and therapeutic effects have never been reported.

It can be noted that appropriate design of nanomaterials[17–19] or nanocomposites with suitable constituents tunes the sustained delivery and doses of drugs for various treatment procedures.[20–22] Depending on the functional behaviour of GO the effective delivery of drug can also be varied. Furthermore, photodynamic therapy (PDT) is an efficient approach to kill

[a]School of Biomedical Engineering, Indian Institute of Technology (BHU), Varanasi 221 005, UP, India. E-mail: paik.bme@iitbhu.ac.in; pradip.paik@gmail.com

[b]School of Engineering Sciences and Technology, University of Hyderabad, Hyderabad-500046, Telangana, India. Tel: (+91)-(040) 2313 4457 (O)

cancer cells.[5,6,9,23–25] Another approach to kill the cancer cell is the chemo-photothermal-therapy[26] (*via* redox-responsive chemotherapy effects), where chemotherapy drugs can be attached (or polymerized) with nanotemplate (*e.g.* carbon nanotube, CNTs) along with photo thermal reagent which helps to release chemotherapy drug under NIR irradiation. However, many studies revealed that bare UCN nanoparticles are toxic and it is challenging for clinical trial and required protection of its surface.[27–29] GO has various limitations on releasing the drugs due to its defects[30] and electronic structure.[31] Therefore, in our newly designed composites (UCN@SiO$_2$–GO) the properties of GO and UCN are combined and the toxicity has been reduced with making thin shell of SiO$_2$ on SiO$_2$. Our new composite UCN@SiO$_2$–GO has been made through bio-conjugation and used for drug delivery applications to counter the lack of quantum efficiency of UCN process[32] and to control the sustained release of drugs. Here the toxic surface of UCN has been protected with thin shell of SiO$_2$ (by sol–gel method) which further helps to make the conjugation[33–35] with GO due to presence of –OH (in SiO$_2$) and –COOH/–OH in GO. Thus we have protected the toxic surface of UCN by making shell of SiO$_2$ and conjugated with GO and subsequently accomplished functional properties like NIR tuned sustained delivery[36–38] of drugs, which is one of the important required parameters to decide doses for effective treatment of cancer.[39]

Results and discussion

Synthesis and characterization of UCN NPs, UCN@SiO$_2$ NPs and UCN@SiO$_2$–GO composites

NaYF$_4$:Yb^{3+},Er^{3+} nanoparticles (UCNPs) have been synthesized and characterized using TEM to know its size and morphology. The TEM micrographs of UCNPs are shown in Fig. 1a and the average particle size calculated to be ∼40–50 nm (dia.).

Fig. 1b shows the AFM surface topography image of UCNPs and the average size of the particles is found to be ∼40 nm (dia.) which is matching well with the results obtained from TEM. Further, both the TEM and AFM micrographs are evident that the UCNPs are spherical in shape.

UCNPs were synthesized and coated with SiO$_2$ shell (UCN@SiO$_2$) through the sol–gel synthesis method using TEOS as precursor. TEM studies were performed to confirm the core shell structure of UCN@SiO$_2$. Fig. 2a and b clearly show the formation of SiO$_2$ shell on the UCNPs. The average SiO$_2$ shell thickness on UCNPs is calculated to be *ca.* 10 nm and is of uniform thickness. Fig. S1a† shows the UCNP@SiO$_2$ NPs at higher magnification which clearly further confirms the two UCN@SiO$_2$ NPs are attached together through SiO$_2$ shell formation. Fig. S1b† shows the individual UCN@SiO$_2$ NPs which are mono dispersed and are not attached to each other.

From Fig. S2† the elements present in the UCN@SiO$_2$ NPs are confirmed, and they are Na, Y, F, Yb, Er, Si, and elemental oxygen. The first large peak indicates the carbon element which is appeared from the carbon coating of TEM grid. The corresponding atomic weight percentages of elements are provided in Table S1.†
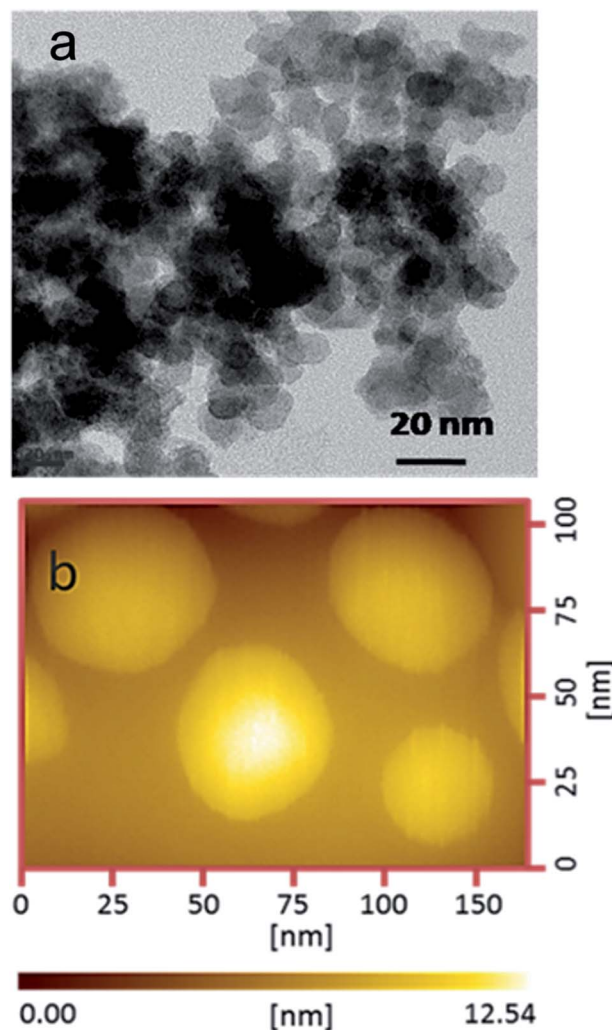

Fig. 1 (a) TEM micrograph and (b) AFM topographic image of UCNPs.

The presence of other elements in the spectra is not identified, *i.e.*, the sample is free from impurities.

Fig. 3a shows the TEM micrograph of UCN@SiO$_2$–GO nanocomposite. In Fig. 3, GO sheet (indicated with arrows) and attached UCN@SiO$_2$ NPs are clearly visible. The UCN@SiO$_2$ NPs are attached onto the GO sheets (indicated with arrows) and are distributed throughout the GO sheet. Fig. 3b shows the UCN@SiO$_2$–GO nanocomposite at a higher magnification. The core and shell of attached UCN@SiO$_2$ NPs are identified clearly from the image. Fig. S3a† shows the composite's image at another region of the sample. More numbers of UCN@SiO$_2$ NPs are seen at the same place. From, TEM image of the core shell structure is clearly seen which is attached onto the surface of the GO sheet. For more clarity, high magnified image is shown in Fig. S3b.† From the image, GO sheets are clearly visible and identified that GO sheet is very thin (1–2 layers). In conclusion, UCN@SiO$_2$ NPs are successfully attached with GO and UCN@SiO$_2$–GO nanocomposite is formed as shown schematically (Scheme 1). The conjugation of UCN@SiO$_2$ NPs with GO further confirmed by FTIR (shown in subsequent section).
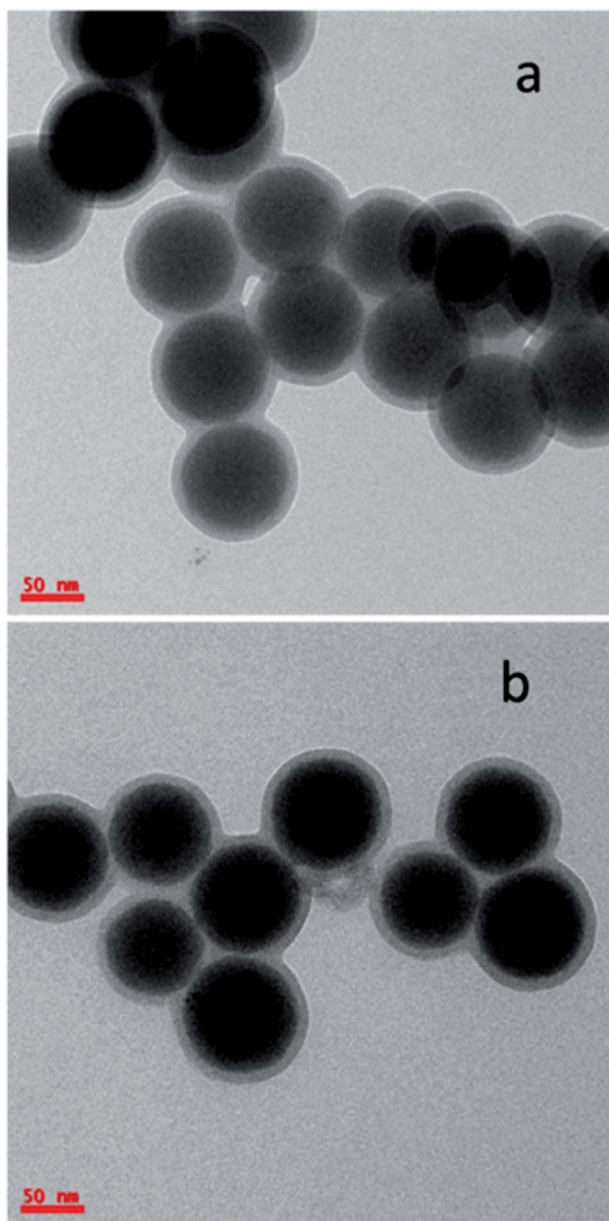
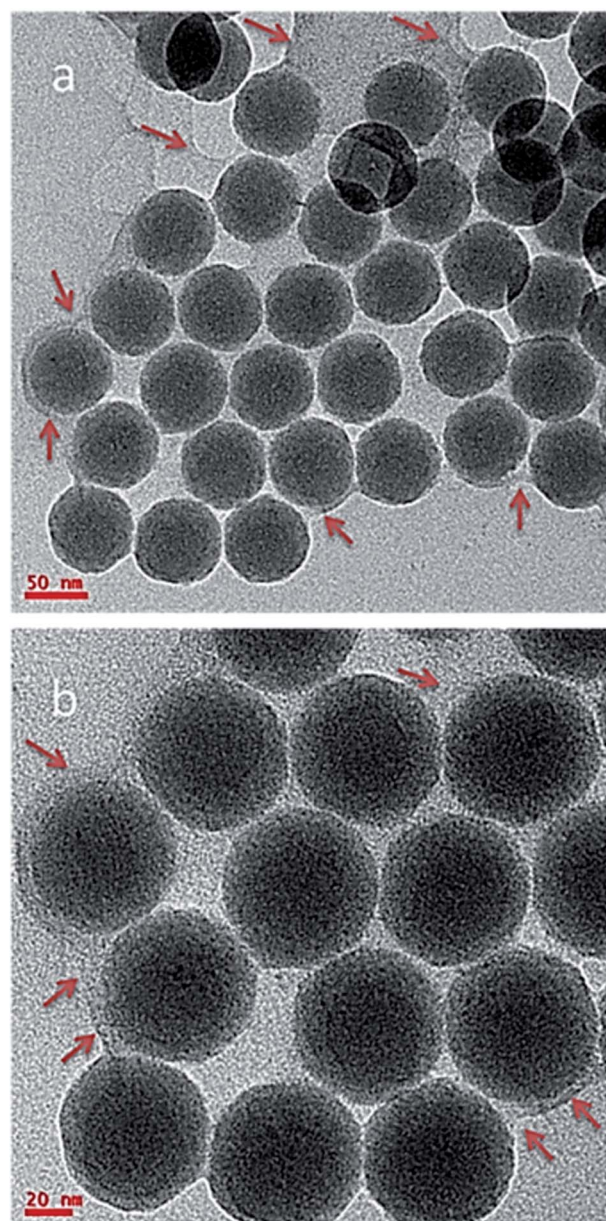Fig. 2 TEM micrographs of (a) core shell UCN@SiO$_2$ NPs (b) at different region.

Fig. 3 TEM micrographs of UCN@SiO$_2$–GO nanocomposite, region (a) at low magnification (b) at high magnification.

FESEM studies have also been performed for UCN@SiO$_2$–GO nanocomposite and the micrographs have been shown in Fig. 4. In Fig. 4, the GO sheets are clearly identified. The UCN@SiO$_2$ NPs (white colour) are uniformly distributed on the entire sheet. To find the uniform distribution of UCN@SiO$_2$ NPs image was collected from the other region of the sample and shown in Fig. S4.† From FESEM micrograph, it is clear that more numbers of GO sheets are corrugated and UCN@SiO$_2$ NPs are attached with the GO sheets. The lateral size of the GO sheets is in micron sized and thickness of the sheets is of 2–3 layers (~1.7 nm).

XRD-studies have been performed for UCNPs, UCN@SiO$_2$ NPs and UCN@SiO$_2$–GO nanocomposite to know their solid state crystal structure (Fig. 5a, b and c, respectively). The

diffraction pattern corresponds to UCNPs, reveals hexagonal crystal structure (JCPDS No. 00-028-1192). For UCNPs, the characteristic peaks are appeared at $2\theta = 17.14°$, $25.96°$, $30.81°$, $34.74°$, $39.67°$, $43.47°$, $46.51°$, $52.10°$, $53.18°$, $53.72°$, $55.26°$, $61.25°$, $62.26°$, $71.03°$, $77.62°$ and $86.71°$ for the corresponding diffraction planes (100), (110), (101), (200), (111), (201), (210), (002), (300), (211), (102), (112), (220), (311), (302) and (321), respectively. The XRD pattern in Fig. 5b corresponds to UCN@SiO$_2$ NPs consists of all the characteristic peaks for UCNPs and a hump at $2\theta = 24°$ appeared which represents the existence of amorphous silica. XRD pattern of UCN@SiO$_2$–GO nanocomposite (Fig. 5c), along with the characteristic peaks of UCNPs and a hump of silica, a peak appeared at $2\theta = 10°$ which corresponds to the (002) diffraction plan for GO. The existence
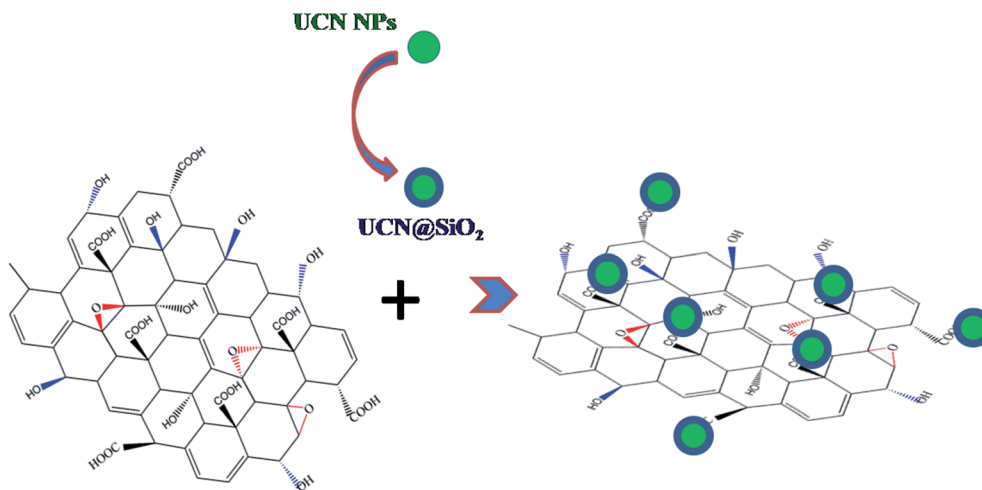
Scheme 1 Schematic showing the concept of making UCN@SiO$_2$–GO conjugated nanocomposite. UCN@SiO$_2$ NPs are conjugated with GO.

of peaks related to these three materials in the XRD pattern of UCN@SiO$_2$–GO nanocomposite (Fig. 5c) confirms the formation of nanocomposite.

The FTIR spectra for the samples have been acquired and shown in Fig. 6. Fig. 6a shows the FTIR spectra for UCNPs. A broad absorption band appeared at 3428 cm^{-1} corresponds to the O–H groups of moisture/–COOH oleic acid used as a capping agent. The absorption bands appeared at 2926 and 2856 cm^{-1} are the characteristic bands for the CH$_2$ of CH$_3$ groups of the oleic acid capped on UCNPs. Band appeared at 1462 cm^{-1} is for the –OH band of carboxylic acid group. Band appeared at 1710 cm^{-1} for C=O stretching. These all confirm for the UCNPs. The spectrum for UCN@SiO$_2$ NPs has been shown in Fig. 6b. The characteristic bands for SiO$_2$ appeared at 1065, 1106, 1210, 812 and 482 cm^{-1} are very much prominent. The broad band appeared at 1632 cm^{-1} O–H groups of moisture and 3126 cm^{-1} associates to O–H groups of SiO$_2$ (SiO–OH). After formation of UCN@SiO$_2$–GO nanocomposite (attaching UCN@SiO$_2$ nanoparticles with GO), the corresponding FT-IR

results have been shown in Fig. 6c. The band appeared at 785, 1068, 1115 and 1628 cm^{-1} represent to the characteristic peaks for SiO$_2$ and 1734 and cm^{-1} corresponds to the aromatic –C=O of GO basal plane. Absorption band appeared at 3437 cm^{-1} corresponds to the O–H groups and the bands appeared at 2934 and 2852 cm^{-1} are for –C–H (–CH$_2$) groups. The existence of the bands i.e., 1734 (C=O), 1633 (–OH) and 1410 cm^{-1} are for functional groups that are related to GO and bands appeared for 1185, 1115, 1068 cm^{-1} correspond to SiO$_2$ and the evidences for the formation of composite.

The fluorescence studies have been performed for the samples of UCNPs, UCN@SiO$_2$ NPs and UCN@SiO$_2$–GO nanocomposite (Fig. 7). For all the materials, three common fluorescence emission bands have been observed. Bands at 526, 545 and 661 nm represent the transitions of photons from $^4H_{11/2}$ to $^4I_{15/2}$, $^4S_{3/2}$ to $^4I_{5/2}$ and $^4F_{9/2}$ to $^4I_{15/2}$ levels of Er,[40,41] respectively. The intensity of the bands is different for three different
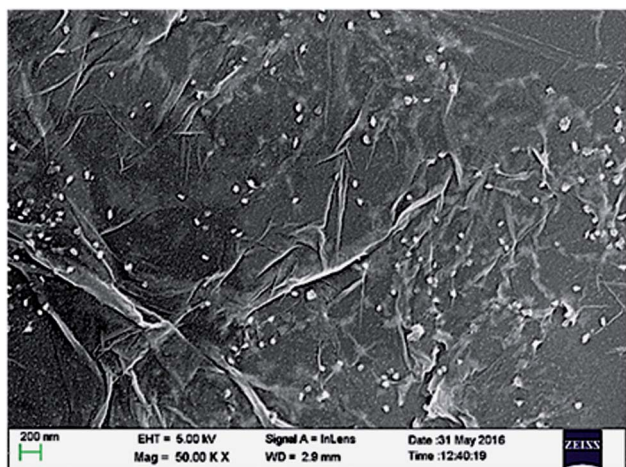
Fig. 4 Representative FESEM micrograph of UCN@SiO$_2$–GO nanocomposite.
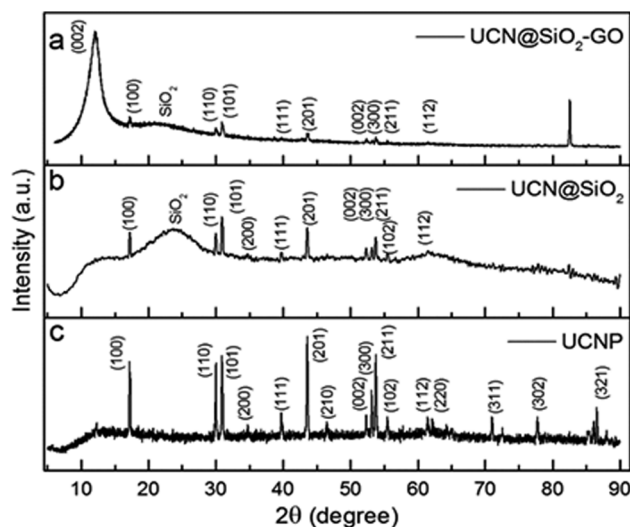
Fig. 5 XRD spectra of UCNPs, UCN@SiO$_2$ NPs and UCN@SiO$_2$–GO nanocomposite.
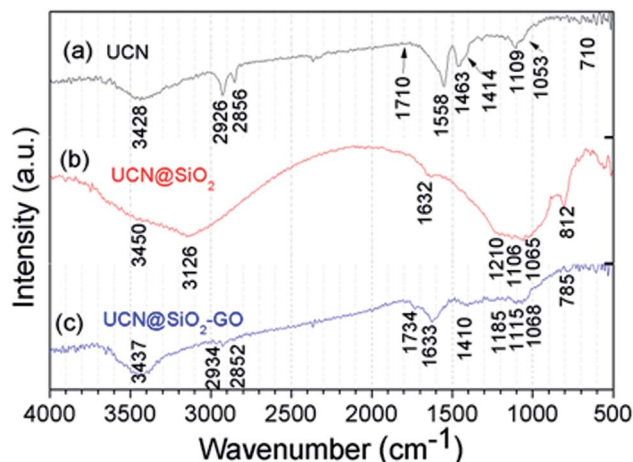
Fig. 6 FTIR spectra of (a) UCNPs, (b) UCN@SiO$_2$ NPs and (c) UCN@SiO$_2$–GO nanocomposite.
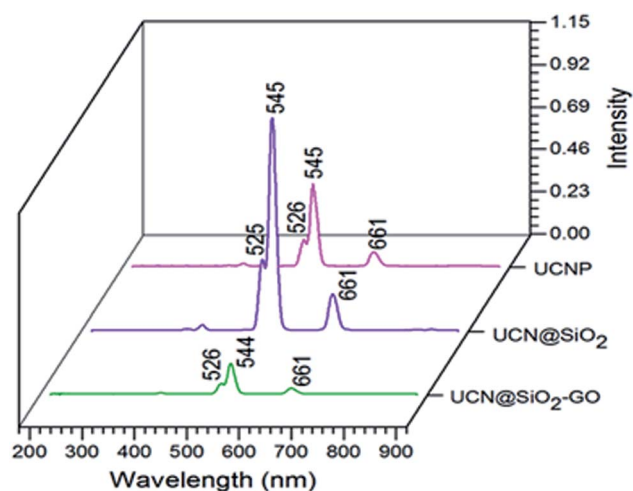

Fig. 7 Fluorescence spectra of UCNPs, UCN@SiO$_2$ NPs and UCN@SiO$_2$–GO nanocomposite.

materials. The intensity of bands of UCN@SiO$_2$ NPs is higher compared to the UCNPs and UCN@SiO$_2$–GO nanocomposite. The reason for relatively low intensity emission might be due to the lesser number of UCN@SiO$_2$ attached onto the GO sheet of UCN@SiO$_2$–GO nanocomposite.

Loading results drug release studies by 980 nm NIR laser irradiation

From the loading results it has been found that out of 50 μm DOX approximately 16 μm loaded in 200 μm of sample (UCN@SiO$_2$–GO), i.e., loading capacity is ∼8%. This loading capacity is also depends on how much UCN@SiO$_2$ attached with GO. To know the applicability of the DOX loaded UCN@SiO$_2$–GO nanocomposite in therapeutic applications, photosensitive drug release studies have been conducted for all three samples (Fig. 8–10). A commonly used anticancer drug DOX was initially loaded in UCNPs, UCN@SiO$_2$ core–shell NPs and UCN@SiO$_2$–GO nanocomposite in individual batch for 24 h (see experimental section for loading and release procedures).

Upon excitation with 980 nm NIR laser various pulse times viz. 1 s, 2 s, 3 s, 5 s, 10 s, 20 s and 30 s irradiation time, the extent of DOX molecules released as shown in Scheme 2 have been calculated from UV-Vis spectra of the supernatant and using the standard release profile the exact amount of DOX released at time to time have been calculated.

Fig. 8 shows the UV-Vis absorption spectra for the DOX release from DOX-UCNPs formulation. The absorption band appeared at 496 nm corresponds to the release of DOX. As the irradiation (NIR 980 nm) time increases from 1 s to 30 s, therefore with NIR 980 nm irradiation with time the amount of DOX released increases as well as the intensity of the UV-Vis absorption bands also increases.

Fig. 9 shows the absorption spectra for the DOX released from DOX-UCN@SiO$_2$ NPs formulation. The characteristic peak for DOX at 496 nm is clearly visible. As the irradiation time (980 nm NIR LASER light) increases from 1 s to 30 s, the amount of DOX released also increased. This is evident from the Fig. 10 that the intensity of the band at 496 nm has increased with time of impulse. Fig. 10 shows the absorption spectra for the release of DOX from DOX-UCN@SiO$_2$–GO nanocomposite formulation.
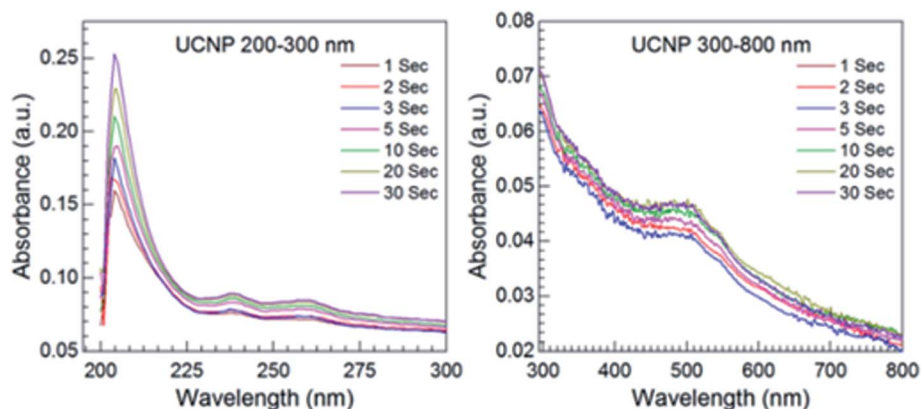

Fig. 8 Time dependent release of DOX studied through UV-Visible absorption spectra for UCNPs.
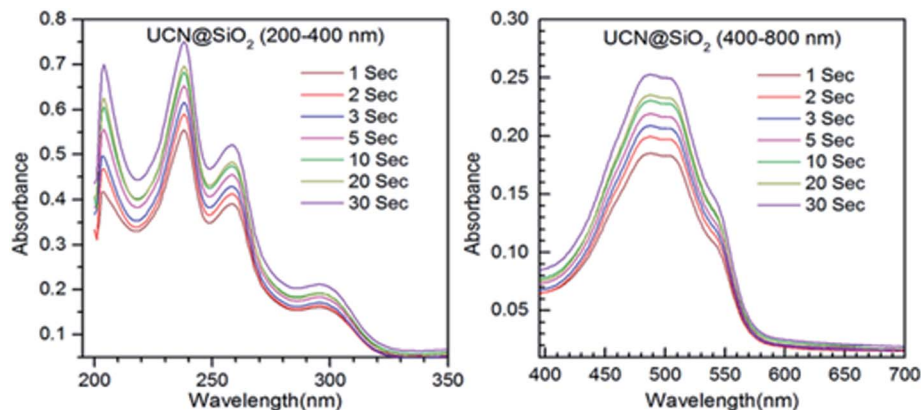
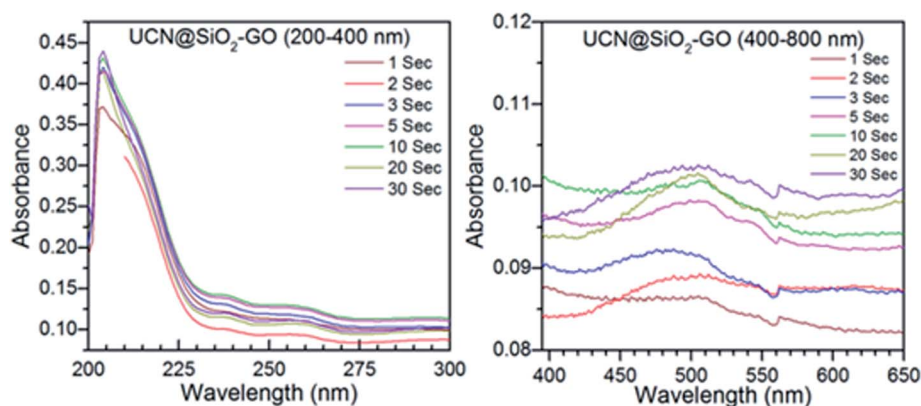**Fig. 9** Time dependent release of DOX studied through UV-Visible absorption spectra for UCN@SiO$_2$ NPs.

Fig. 10 Time dependent release of DOX studied through UV-Visible absorption spectra for UCN@SiO$_2$–GO nanocomposite.

For this nanocomposite a characteristic emission band for DOX at 496 nm is also observed. However, the intensity of the absorption band due to the DOX released is less compared to the DOX released from DOX-UCN@SiO$_2$ NPs formulation.

The decrease in the intensity of band at 496 nm of DOX at a particular impulse is observed which might be due to the limited number of attached UCN@SiO$_2$ NPs to the GO sheet. As the irradiation time of 980 nm laser increased the amount of drug released has found to be also increased for this material (from the intensity of the peak).

Extent of DOX released from UCNPs, UCN@SiO$_2$ NPs and UCN@SiO$_2$–GO nanocomposite

It is worth mentioning that the ratio of drug to nanomaterials was maintained at 1 : 1 during incubation period. A fixed amount of sample (200 μg) and a fixed amount of DOX (200 μg) has been taken for loading separately into three different samples *e.g.*, UCN, UCN@SiO$_2$ and UCN@SiO$_2$–GO as it has been explained in the experimental section. With different 980 nm NIR pulse times the release of DOX has been controlled as it is shown in Scheme 1.

The amount of DOX released (in μg) has been calculated (Table 1). The release kinetics with different pulse times have also been shown in Fig. 11. It is obvious that with increase in

pulse time the extent of DOX released also increases for all three samples. For UCNPs, a continuous release with pulse is observed. For UCN@SiO$_2$, up to 5 s pulse a rapid release of DOX is observed, whereas the release at higher pulse time, the rate of release becomes slow. For UCN@SiO$_2$ nanoparticles, up to the initial 5 s pulse, release is as comparable to the 'Burst effect of release'. For UCN@SiO$_2$–GO nanocomposite, combination effects of release of UCNPs plus UCN@SiO$_2$ nanoparticles have been observed. Up to 2 s pulse, a 'Burst effect type of release' and up to 8 s, a moderately slow release followed by a slow release at higher impulse time have been observed. For UCN@SiO$_2$–GO nanocomposite, this unique nature of release behaviour is observed due to the combinational effects of UCNPs, GO and SiO$_2$ (in UCN@SiO$_2$–GO) and due to the effective electrostatic forces of interactions act between DOX molecules and UCN@SiO$_2$–GO composite. From Fig. 10 and Table 1, it is obvious and can be concluded that for faster and more extent of release, sample UCN@SiO$_2$ NPs is effective. Whereas, for slow and controlled release sample UCN@SiO$_2$–GO nanocomposite is effective for therapeutic applications.

Biocompatibility studied with MTT assay

To find out the applicability of any materials it must pass the quality control and therefore the cellular toxicity study is very
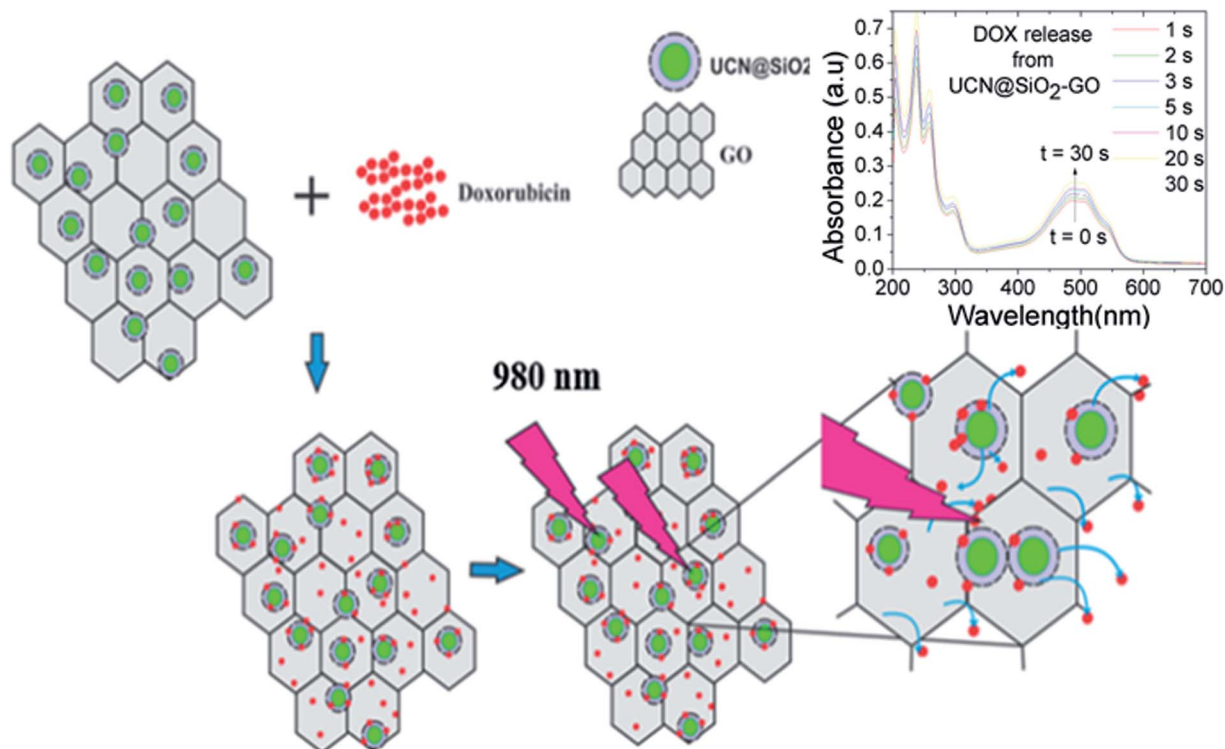
Scheme 2 Represents the procedure and mechanism of control release of DOX from UCN@SiO$_2$–GO. Release of DOX has been controlled by 980 nm NIR laser pulse.

important. To qualify this criteria we have studied the biocompatibility of UCNPs, UCN@SiO$_2$ core–shell NPs and UCN@SiO$_2$–GO nanocomposite using model noncancerous cell line (HEK293 cells) and with model human carcinoma cell lines *e.g.*, HepG2. by MTT assay as it is mentioned in the experimental section. Various concentrations of each samples were taken *e.g.*, 0, 10, 25, 50, 100 and 200 μg mL^{-1} with fixed number of cells ~5 × 10^3. From the Fig. 12(a) and (b) it is clearly evident that UCN NPs are toxic for both the noncancerous cell line (HEK293 cells) as well as human carcinoma HepG2 cells. With the formation of shell on UCN NPs (*i.e.*, for UCN@SiO$_2$ NPs) the toxicity level can be reduced. Furthermore, UCN@SiO$_2$–GO nanocomposite also has found biocompatible (Fig. 12). However, the extent of toxicity of UCN@SiO$_2$–GO depends on the amount of GO attached with UCN@SiO$_2$ NPs. GO alone is toxic as it has mentioned earlier, and that depends on the extent of functional groups attached with the GO sheet. In conclusion, UCN@SiO$_2$ core–shell NPs and UCN@SiO$_2$–GO nanocomposite prepared in this work are biocompatible in nature.

In vitro killing of cancer cells: efficiency studied with DOX loaded UCN@SiO$_2$–GO nanocomposite formulation

Controlled release behaviour (Fig. 11) and biocompatible results (Fig. 12) provoked us to use UCN@SiO$_2$–GO nanocomposite for the therapeutic applications. Therefore, we have used DOX loaded UCN@SiO$_2$–GO nanocomposite formulation to check the killing efficiency of human carcinoma HepG2 cells. *In vitro* killing efficiency on HepG2 using UCN@SiO$_2$–GO nanocomposite loaded with DOX (loaded sample designated as

formulations) have been studied with 980 nm NIR irradiation for the different pulse durations such as, 1 s, 2 s, 3 s and 5 s by MTT assays as the procedure has been mentioned in the experimental section. These experiments were performed up to maximum 5 s pulse because most of the DOX molecules released from DOX-UCN@SiO$_2$–GO formulation have been found to be at 5 s with 980 nm NIR pulse and longer pulse degradation of DOX occurs. Furthermore, by short period of irradiation of NIR we could *ca.* avoided the unwanted direct interaction of laser and HepG2 cells. Fig. 13 shows the cell killing efficiency of the formulation. During study we have taken zero weight formulation with zero second pulse as control for each concentration of formulation. Herein, we have taken 0, 25, 50, 100 and 200 μg mL^{-1} formulations and they have been excited with 0 s, 1 s, 2 s, 3 s and 5 s pulse and the killing efficiency on irradiation with NIR 980 nm have been shown in Fig. 13. From the figure it is evident that with up to 5 s pulse of laser irradiation has a minor (up to 9.8%) effects on cells. However, as the concentration of formulation increases for each pulse of laser cell death increase irrespective to the amount of formulation. As an example, as the amount of formulation increases from 25 μg mL^{-1} to 200 μg mL^{-1} at 1 s pulse the cell death also increases from 92 ± 6.1% to 61 ± 9.2%, respectively. Similarly, as concentration increases from 25 μg mL^{-1} to 200 μg mL^{-1} at 2 s, 3 s, 5 s pulses the cell death also increases from 88.2 ± 8.3 to 52.4 ± 9.2%, 82.5 ± 9.52% to 43.2 ± 8.52% and 79.1 ± 7.25% to 41.2 ± 8.23%, respectively. These observations suggested that DOX-UCN@SiO$_2$–GO formulation on NIR 980 nm irradiation with different pulse times is effective for control release of DOX as well as is effective in killing the cancer cells.

Table 1 Amount of drug released for various pulse time exposures of the samples UCNPs, UCN@SiO₂ NPs and UCN@SiO₂–GO nanocomposite when fixed amount of DOX is loaded
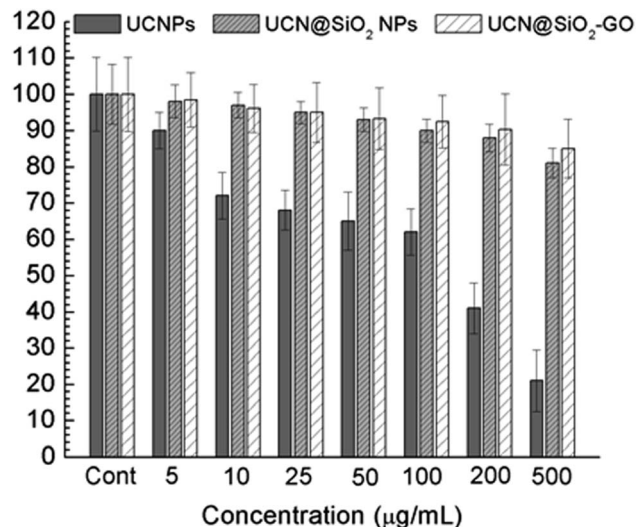
Pulse time (sec)	Amount of DOX released (μg) from different formulations		
	UCN NPs	UCN@SiO$_2$ NPs	UCN@SiO$_2$–GO composite
1	6.86587	28.68	10.29
2	6.92417	31.02	10.59
3	6.92417	31.83	13.97
5	7.05245	33.25	15.40
10	7.11076	35.92	15.58
20	7.18073	36.99	14.15
30	7.21572	39.48	14.68
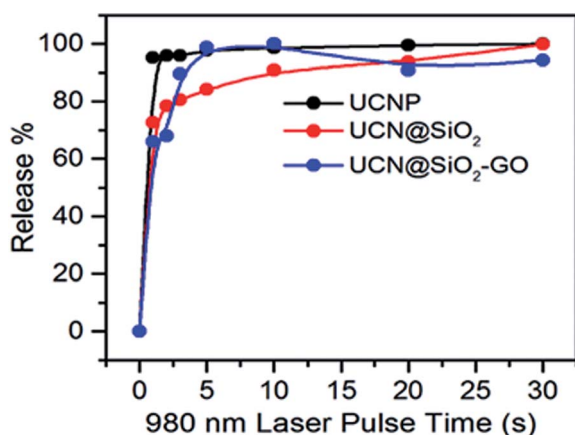
Fig. 11 DOX release profile with different pulse time period for UCNPs, UCN@SiO₂ NPs, UCN@SiO₂–GO nanocomposite.
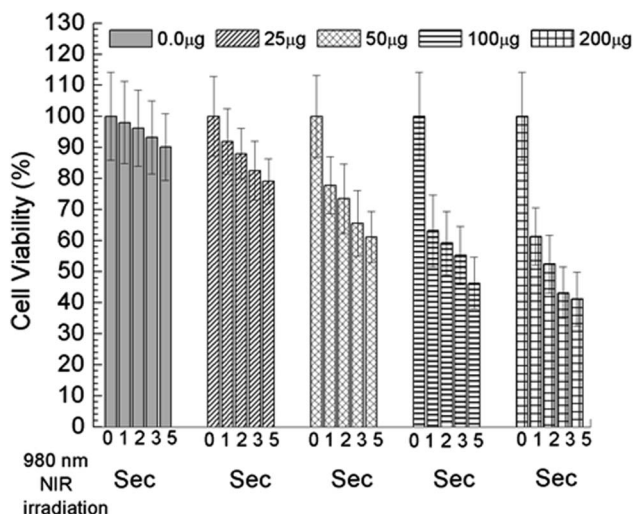
Fig. 13 *In vitro* killing of cancer cells studied with DOX loaded UCN@SiO₂–GO nanocomposite formulation for 10, 25, 50, 100 and 200 μg mL^{-1} and 980 nm NIR laser irradiation for the different pulse, 0 s, 1 s, 2 s, 3 s and 5 s. Study performed with model human carcinoma cell lines (HepG2). Pulse 0 s is control for all.

Experimental

Synthesis of GO

GO has been synthesized through modified Hummer's method with prior ultrasonication as mentioned in our earlier reported work.[30]

Synthesis of upconversion (UCN) nanoparticles (NPs)

Upconversion nanoparticles were synthesized using hydrothermal method that has been described as follows. Aqueous solutions (1 M each) of YCl₃, YbCl₃ and ErCl₃ were prepared. 0.8 mL of YCl₃ and 0.2 mL of YbCl₃ and 0.2 mL of ErCl₃ were added into a 50 mL round bottle flux (RB). This mixture was heated at 100–110 °C and evaporated the water. Then, this mixture was cooled down to room temperature (RT). The octadecene (15 mL) and oleic acid (6 mL) were added and slowly heated to 140–160 °C until the solid particles get dissolved. Afterwards, NaOH (0.1 g in 5 mL methanol) and NH₄F (0.14 g in 5 mL methanol) were added to the RB and kept it for 30 min at room temperature. Then, it was slowly heated to 100 °C under Ar gas environment. Further, the RB was heated up to 300 °C for 1.5 h and then cooled to room temperature. Finally the white solid product was separated using acetone and cyclohexane followed by centrifugation. The precipitation was dispersed in 50 mL cyclohexane for storage.

Synthesis of core–shell UCN@SiO₂ NPs

1 mL UCN nanoparticles cyclohexane solution was taken in a reaction vessel and 4 mL additional cyclohexane was added to it for dilution. 50 μL Igepal CO-50 was added to the reaction vessel and sonicated for 10 min. After that, 20 μL Igepal CO-50 and 40 μL NH₄OH was added to it, sealed with Teflon tape and

Fig. 12 *In vitro* Cell viability measured by MTT assay, (a) UCNPs, (b) UCN@SiO₂ core–shell NPs and (c) UCN@SiO₂–GO nanocomposite. Study performed with model human carcinoma cell lines (HepG2).

sonicated for 20 min till the transparent solution forms. Then, 20 μL TEOS was added to it and stirred for 2 days on the orbital shaker. Acetone was added to the reaction mixture to precipitate the particles. This product was washed with 1 : 1 ethanol and water solution for 5 times, and then centrifuged at 10 000 rpm and the precipitates were collected.

Synthesis of UCN@SiO$_2$–GO nanocomposite

This nanocomposite was synthesized by a simple solution mixing method. First, 5 mg of UCN@SiO$_2$ NPs were dispersed in 5 mL of distilled water and sonicated for 5 min. Then 1 mg of GO was taken into 5 mL of distilled water and sonicated until the solution becomes light brown. Then these solutions were mixed and stirred at 50 °C for 24 h. The resultant solution was centrifuged at 9000 rpm and the precipitate was collected and heated at 90 °C for overnight. Then the final powder was collected.

DOX loading and release from UCN, UCN@SiO$_2$ and UCN@SiO$_2$–GO nanocomposite

The loading studies were carried out using an anticancer drug *i.e.* DOX. Wherein, the weight ratio of DOX to nanomaterials was maintained 1 : 1 for all the samples. 200 μg of sample was incubated with 50 μg of DOX solution and the mixture was kept in dark for 24 h. After 24 h, the loaded materials were separated from the free DOX by centrifugation (at 12 000 rpm). Further, excess of bound drug was removed by washing with PBS (0.1 M, pH ∼ 7.2). The loaded nanomaterials were then subjected to freeze drying (−80 °C) to obtain dry loaded samples.

To study the release, the DOX loaded samples (formulations) were dispersed in PBS (pH ∼7.2) by using UV-Vis spectroscopy, wherein λ_{max} for the DOX was considered at 496 nm. Initially 3 mL of release medium PBS (pH ∼ 7.2) was used as working solution. At first, DOX loaded formulations were dispersed and then systematically irradiated with 980 nm NIR LASER for the different pulse durations such as 1 s, 2 s, 3 s, 5 s, 10 s, 20 s and 30 s. For every irradiation time of LASER, simultaneously UV-Vis spectrum for the corresponding release media was recorded. This step was repeated thrice for every sample for every single irradiation with NIR 980 nm laser. The amount of drug released from the DOX loaded samples was calculated by using DOX standard plot.

In vitro biocompatibility and NIR irradiation based release and killing efficiency of cancer cells

In vitro biocompatibility of UCN NPs, UCN@SiO$_2$ NPs and UCN@SiO$_2$–GO nanocomposite before loading of DOX (unloaded) were conducted using model noncancerous cell line HEK293 cells and with model human carcinoma cell lines *e.g.*, HepG2. Experiments were conducted according to our previously reported methods (biological cell samples were obtained from School of Life Sciences, University of Hyderabad, India).[42] In brief, 3-(4,5-dimethylthiazol-2-yl)-2,5-diphenyl-tetrazolium bromide (MTT) assays were conducted in 96 well culture plates using growing cell lines. 100 μL of medium containing ∼5 × 10^3 cells were taken in each well of 96 well plates and the

plate was incubated in CO$_2$ incubator with 5% CO$_2$ injection at 37 °C for 24 h. Next day the various concentrations of each sample were added to each well separately to get final concentration of 0, 10, 25, 50, 100 and 200 μg mL^{-1}, respectively. Three sets were prepared for each concentration and for each sample to minimize the errors. 100 mL of medium was used as a control sample. Then the cells were incubated in CO$_2$ incubator (5%) for 24 h at 37 °C. After 24 h incubation 20 μL of 5 mg mL^{-1} MTT prepared in 1× PBS was added to each well in dark and incubated in CO$_2$ incubator (5%) for 3 h at 37 °C. Then 50 μL of PBS was added to each well and incubated for 5 min and then the absorbance was recorded at 570 nm with microplate reader (BioTek). Cells viability at each concentration was calculated using the eqn (1):

$$\text{Viability (\%)} = [(\text{ABST})/(\text{ABSC})] \times 100 \quad (1)$$

where the ABST and ABSC are the absorbance of treated and control cultures, respectively at 570 nm. It can be noted that same culture medium was taken for various experiments to reduce the errors.

In vitro 980 NIR irradiation based release and killing efficiency of cancer cells

In vitro killing efficiencies of model human carcinoma cell lines *e.g.*, HepG2 using UCN@SiO$_2$–GO nanocomposite loaded with DOX (formulations) have been studied with 980 nm NIR laser irradiation for the different pulse durations such as, 1 s, 2 s, 3 s and 5 s. MTT assays were conducted to find out the efficacy of the formulations to kill the cancer cells. 100 μL of medium containing ∼5 × 10^3 cells were taken in each well of 96 well plates and the plate was incubated in CO$_2$ incubator with 5% CO$_2$ injection at 37 °C for 24 h. Next day 200 μg (sample)-equivalent formulation mL^{-1} (DOX loaded UCN NPs, UCN@SiO$_2$ NPs and UCN@SiO$_2$–GO nanocomposite), for each formulation were added to each well separately (to achieve an equivalent weight of release of DOX as mentioned in Table 1 with respect the irradiation 980 nm NIR pulse time). Three experimental sets were prepared for each sample-formulation and for each pulse of NIR 980 nm irradiation. Equivalent volume of media containing cultured cells without formulation was taken as control. Then the cells were incubated in CO$_2$ incubator (5%) for 24 h at 37 °C. After 24 h incubation, 20 μL of 5 mg mL^{-1} MTT prepared in 1× PBS was added to each well in dark and incubated in CO$_2$ incubator for another 3 h. Then 50 μL of PBS was added to each well and incubated for 5 min and then the absorbance was recorded at 570 nm with microplate reader. Finally cells viability/killing efficiency at each formulation with each irradiation time was calculated as mentioned in the earlier section (eqn (1)). Efficiency of killing of formulations were studied with 1 s, 2 s, 3 s and 5 s 980 NIR irradiation, because most of the DOX released within 5 s irradiation of 980 nm NIR.

Conclusions

The photosensitive delivery of UCN@SiO$_2$–GO nanocomposite has been studied and compared with UCNPs and UCN@SiO$_2$

NPs. Three materials showed green fluorescence with the excitation of 980 nm NIR laser due to the embedded UCNPs. The release of the drug DOX has been studied for all the three materials, after incubation and loading of DOX for 24 h. The increase in the laser irradiation time from 1 s to 30 s leads the increase in the amount of drug released. The attachment of core–shell UCN@SiO$_2$ NPs to GO sheets renders UCN@SiO$_2$–GO nanocomposite as a multifunctional agent for drug delivery, imaging and photodynamic therapy. The GO sheets play a vital role in attaching the biomolecules with this nanocomposite since GO has been proven to be a biocompatible materials up to certain concentration. SiO$_2$ is also known to be a biomaterial which avoids the toxicity of UCNPs by forming shell over them. For the faster and more release of DOX the sample UCN@SiO$_2$ nanoparticles is effective, whereas, for the slow release of the DOX, UCN@SiO$_2$–GO nanocomposite is effective one. From the *in vitro* studies it can be concluded that UCN@SiO$_2$–GO nanocomposite is biocompatible and could be an effective material for the therapeutic applications such as for controlled killing of cancer cells. Additional *in vivo* study is required for effective use of this multifunctional UCN@SiO$_2$–GO nanocomposite in delivery and therapeutic applications which is the future scope of this work and is under investigation.

Conflicts of interest

There are no conflicts to declare.

Acknowledgements

References

1 F. Auzel, *Chem. Rev.*, 2004, **104**, 139–174.

2 D. Lee, K. Jeong, X. Luo, G. Kim, Y. Yang, X. Chen, S. Kim and J. Yoon, *J. Mater. Chem. B*, 2018, **6**, 2541–2546.

3 D. E. J. G. J. Dolmans, D. Fukumura and R. K. Jain, *Nat. Rev. Cancer*, 2003, **3**, 380.

4 D. J. Burgess, *Nat. Rev. Cancer*, 2012, **12**, 737.

5 A. Bansal, F. Yang, T. Xi, Y. Zhang and J. S. Ho, *Proc. Natl. Acad. Sci. U. S. A.*, 2018, **115**, 1469.

6 Z. Lv, H. Wei, Q. Li, X. Su, S. Liu, K. Y. Zhang, W. Lv, Q. Zhao, X. Li and W. Huang, *Chem. Sci.*, 2018, **9**, 502–512.

7 C. Ding, J. Wang, W. Zhang, X. Pan, Z. Zhang, W. Zhang, J. Zhu and X. Zhu, *Polym. Chem.*, 2016, **7**, 7370–7374.

8 Z. Ruan, L. Liu, L. Fu, T. Xing and L. Yan, *Polym. Chem.*, 2016, **7**, 4411–4418.

9 N. M. Idris, M. K. Gnanasammandhan, J. Zhang, P. C. Ho, R. Mahendran and Y. Zhang, *Nat. Med.*, 2012, **18**, 1580.

10 T. Jing, L. Fu, L. Liu and L. Yan, *Polym. Chem.*, 2016, **7**, 951–957.

11 X. Sun, Z. Liu, K. Welsher, J. T. Robinson, A. Goodwin, S. Zaric and H. Dai, *Nano Res.*, 2008, **1**, 203–212.

12 M. de Sousa, L. A. Visani de Luna, L. C. Fonseca, S. Giorgio and O. L. Alves, *ACS Appl. Nano Mater.*, 2018, **1**, 922–932.

13 K. Muthoosamy, R. G. Bai and S. Manickam, *Curr. Drug Delivery*, 2014, **11**, 701–718.

14 Y. Xin, M. Yin, L. Zhao, F. Meng and L. Luo, *Cancer Biol. Med.*, 2017, **14**, 228–241.

15 T. Li, S. D. Christensen, P. H. Frankel, K. A. Margolin, S. S. Agarwala, T. Luu, P. C. Mack, P. N. Lara, Jr and D. R. Gandara, *Invest. New Drugs*, 2012, **30**, 741–748.

16 A. Raza, U. Hayat, T. Rasheed, M. Bilal and H. M. N. Iqbal, *J. Mater. Res. Technol.*, 2018, DOI: 10.1016/j.jmrt.2018.03.007.

17 A. K. Yamala, V. Nadella, Y. Mastai, H. Prakash and P. Paik, *Nanoscale*, 2017, **9**, 14006–14014.

18 S. Afroz, H. Medhi, S. Maity, G. Minhas, S. Battu, J. Giddaluru, K. Kumar, P. Paik and N. Khan, *Nanoscale*, 2017, **9**, 14641–14653.

19 V. B. Kumar, K. Kumar, A. Gedanken and P. Paik, *J. Mater. Chem. B*, 2014, **2**, 3956–3964.

20 P. T. Wong, S. Tang, J. Mukherjee, K. Tang, K. Gam, D. Isham, C. Murat, R. Sun, J. R. Baker and S. K. Choi, *Chem. Commun.*, 2016, **52**, 10357–10360.

21 T. J. Sill and H. A. von Recum, *Biomaterials*, 2008, **29**, 1989–2006.

22 A. K. Gupta and M. Gupta, *Biomaterials*, 2005, **26**, 3995–4021.

23 T. J. Dougherty, C. J. Gomer, B. W. Henderson, G. Jori, D. Kessel, M. Korbelik, J. Moan and Q. Peng, *JNCI, J. Natl. Cancer Inst.*, 1998, **90**, 889–905.

24 T. J. Dougherty, J. E. Kaufman, A. Goldfarb, K. R. Weishaupt, D. Boyle and A. Mittleman, *Cancer Res.*, 1978, **38**, 2628–2635.

25 J. P. Celli, B. Q. Spring, I. Rizvi, C. L. Evans, K. S. Samkoe, S. Verma, B. W. Pogue and T. Hasan, *Chem. Rev.*, 2010, **110**, 2795–2838.

26 D. Wang, Y. Ren, Y. Shao and L. Meng, *Polym. Chem.*, 2017, **8**, 6938–6942.

27 A. Gnach, T. Lipinski, A. Bednarkiewicz, J. Rybka and J. A. Capobianco, *Chem. Soc. Rev.*, 2015, **44**, 1561–1584.

28 A. Monks, E. D. Harris, A. Vaigro-Wolff, C. D. Hose, J. W. Connelly and E. A. Sausville, *Invest. New Drugs*, 2000, **18**, 95–107.

29 A. Jimeno, M. A. Rudek, T. Purcell, D. A. Laheru, W. A. Messersmith, J. Dancey, M. A. Carducci, S. D. Baker, M. Hidalgo and R. C. Donehower, *Cancer Chemother. Pharmacol.*, 2008, **61**, 423–433.

30 K. S. Kumar, S. Pittala, S. Sanyadanam and P. Paik, *RSC Adv.*, 2015, **5**, 14768–14779.

31 D. R. Dreyer, S. Park, C. W. Bielawski and R. S. Ruoff, *Chem. Soc. Rev.*, 2010, **39**, 228–240.

32 M. D. Wisser, S. Fischer, C. Siefe, A. P. Alivisatos, A. Salleo and J. A. Dionne, *Nano Lett.*, 2018, **18**, 2689–2695.

33 X. Zhao, T. Shang, X. Zhang, T. Ye, D. Wang and L. Rei, *Nanoscale Res. Lett.*, 2016, **11**, 451.

34 S. Santra, P. Zhang, K. Wang, R. Tapec and W. Tan, *Anal. Chem.*, 2001, **73**, 4988–4993.

35 U. Kostiv, I. Kotelnikov, V. Proks, M. Šlouf, J. Kučka, H. Engstová, P. Ježek and D. Horák, *ACS Appl. Mater. Interfaces*, 2016, **8**, 20422–20431.

36 C. Pinese, J. Lin, U. Milbreta, M. Li, Y. Wang, K. W. Leong and S. Y. Chew, *Acta Biomater.*, 2018, **76**, 164–177.

37 X. Niu, Z. Liu, F. Tian, S. Chen, L. Lei, T. Jiang, Q. Feng and Y. Fan, *Sci. Rep.*, 2017, **7**, 45655.

38 N. A. Fletcher and M. D. Krebs, *RSC Adv.*, 2018, **8**, 8999–9005.

39 R. Lupertz, W. Watjen, R. Kahl and Y. Chovolou, *Toxicology*, 2010, **271**, 115–121.

40 M. A. Chamarro and R. Cases, *J. Lumin.*, 1990, **46**, 59–65.

41 M. Shojiya, M. Takahashi, R. Kanno, Y. Kawamoto and K. Kadono, Upconversion luminescence of Er^{3+} in CdX_2 system glasses (X = Cl, Br, I), *Appl. Phys. Lett.*, 1995, **67**, 2453–2455.

42 C. Amgoth, G. Dharmapuri, A. M. Kalle and P. Paik, *Nanotechnology*, 2016, **27**, 125101.